ACS OMEGA

http://pubs.acs.org/journal/acsodf

Article

Adsorption Separation of Cr(VI) from a Water Phase Using Multiwalled Carbon Nanotube-Immobilized Ionic Liquids

Lihan Sun,[†] Mengru Wang,[†] Wei Li, Sha Luo, Yan Wu, Chunhui Ma,* and Shouxin Liu*

Cite This: *ACS Omega* 2020, 5, 22827−22839

Read Online

ACCESS | Metrics & More | Article Recommendations | Supporting Information

ABSTRACT: Three types of multiwalled carbon nanotubes (MWCNTs, MWCNTs-OH, and MWCNTs-COOH) were used as carriers and five types of ionic liquids (ILs) were immobilized on each carrier by an impregnation method. Boehm titration, Fourier-transform infrared spectroscopy, X-ray photoelectron spectroscopy, specific surface area analysis by the Brunauer−Emmett−Teller method, and thermogravimetric analysis were performed to investigate [C4mim]HSO_4 adsorption by the MWCNTs. The MWCNT-immobilized IL was used for Cr(VI) removal from a water phase. The adsorption properties of MWCNTs-COOH-immobilized [C4mim]HSO_4 were investigated by single-factor analysis. The results showed that the Cr(VI) removal rate was 52.14% and the adsorption capacity was 31.29 mg/g. The optimum adsorption conditions were as follows: initial Cr(VI) concentration, 60 mg/L; adsorbent dosage, 50 mg; pH 2.0; adsorption temperature 40 °C; and adsorption time, 200 min. Adsorption isotherm data fitted the Freundlich model, which indicates that the adsorption process was in line with the multimolecular layer adsorption theory. The Cr(VI) adsorption behaviors of the three adsorbents were consistent with a pseudo-second-order dynamic model. Thermodynamic analysis of the reaction systems was also performed. The Cr(VI) removal rates of MWCNTs-3, MWCNTs-OH-3, and MWCNTs-COOH-3 were 27.97, 9.39, and 7.34% lower than the initial removal rates after five cycles.

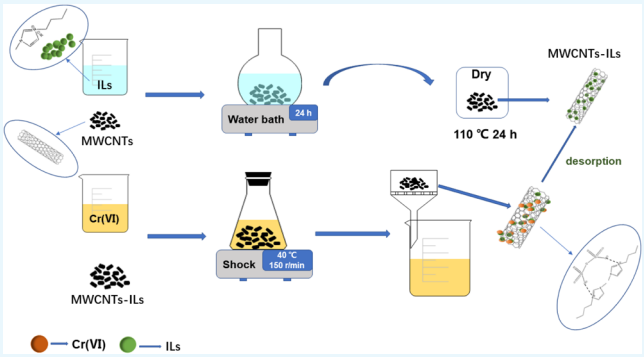

1. INTRODUCTION

Water is a key natural resource for human survival and development. Problems are caused by uneven distribution of water resources and pollution caused by human activities. Chromium is one of the main heavy-metal pollutants in environmental water systems.[1] The sources of chromium pollution are mining and smelting of chromium ore, and the use of chromium compounds in areas such as offset printing, electroplating, alloys, dyes, and agriculture.[2,3] Chromic compounds are not self-degradable and long-term accumulation in humans and other organisms occurs readily. Chromium is carcinogenic in humans.[4,5]

Various methods, e.g., chemical,[6] electrolytic,[7] ion-exchange,[8] membrane separation,[9] biological,[10] and adsorption,[11] are currently used for removal of heavy metals from water. In recent years, membrane separation technology has been used to remove heavy metals. Sellami et al.[9] used new polymer inclusion membranes to remove Cr(VI) in aqueous solutions; the results showed that the chromium removal rate reached 97%. However, membrane separation processes are complex, membranes are easily polluted, and maintenance costs are high. Adsorption methods are operationally simple, a wide range of adsorbents are available and they can be reused.[12] Adsorption techniques are, therefore, widely used in domestic sewage treatment. Among the many types of available adsorbents,[13] the most common include multiwalled carbon nanotubes (MWCNTs),[14] diatomites,[15] activated carbon,[16] and biomass adsorbents.[17] MWCNTs have attracted much attention because of their super-high strength, ductility, large specific surface areas, and complex pore structures.[18,19] However, MWCNTs have some limitations. They are hydrophobic materials with high surface activities, therefore their homogeneous dispersion in water phases is difficult and they agglomerate easily.[20,21] MWCNTs are therefore usually modified by ionic liquid (IL) immobilization to enable their effective and wide use in treatment of polluted water.[22]

ILs are molten salts that consist of cations and anions, and are liquid at or near room temperature.[23] Common ILs generally consist of fluoride anions and alkylimidazolium cations.[24] ILs have many advantages over traditional organic and inorganic solvents; these include good thermal stability, conductivity, and solubility, low steam pressure, regulation,

Received: May 1, 2020
Accepted: August 18, 2020
Published: September 1, 2020

https://dx.doi.org/10.1021/acsomega.0c02016
ACS Omega 2020, 5, 22827−22839

wide electrochemical windows, and low toxicity.[25−28] Furthermore, ILs can be recycled, are cheap, and meet the requirements of green chemistry.[29,30] They are widely used in areas such as electrochemistry,[31] organic chemical reactions,[32] separation and purification, and synthesis of inorganic nanomaterials.[33]

In this study, we used an impregnation method to immobilize ILs on MWCNTs. The obtained materials were characterized by Boehm titration, Fourier-transform infrared (FT-IR) spectroscopy, X-ray photoelectron spectroscopy (XPS), the Brunauer−Emmett−Teller (BET) method, and thermogravimetry-differential thermal gravimetry (TG-DTG). The samples were used for Cr(VI) adsorption in an aqueous solution and the recycling capacities of the samples were evaluated. The adsorption isotherms, adsorption kinetics, and adsorption thermodynamics were investigated. The results of this study will promote the use of MWCNTs in sewage treatment.

2. RESULTS AND DISCUSSION

2.1. Effect of IL Addition. The adsorbents that were prepared in this study are listed in Table 1. The data in Table 2 show that the weight of MWCNT-immobilized ILs stabilized at an IL dosage of 0.5 g. This is because the amounts of available pores and binding sites on the MWCNTs became limited as the IL amount increased; binding sites were filled and the amount of IL that could be adsorbed reached saturation. The presence of van der Waals forces among the MWCNTs was due to the large aspect ratio and the nano effect of MWCNTs. An IL dosage of 0.5 g was selected.

Table 1. Processing Number of MWCNTs

number	sample name	named number
1	[C4mim]CH_2-C_6H_4-HSO_3/MWCNTs	MWCNTs-1
2	[C4mim]CH_2-HSO_3/MWCNTs	MWCNTs-2
3	[C4mim]HSO_4/MWCNTs	MWCNTs-3
4	[C4mim]OH/MWCNTs	MWCNTs-4
5	[C4mim]Ac/MWCNTs	MWCNTs-5
6	[C4mim]CH_2-C_6H_4-HSO_3/MWCNTs-OH	MWCNTs-OH-1
7	[C4mim]CH_2-HSO_3/MWCNTs-OH	MWCNTs-OH-2
8	[C4mim]HSO_4/MWCNTs-OH	MWCNTs-OH-3
9	[C4mim]OH/MWCNTs-OH	MWCNTs-OH-4
10	[C4mim]Ac/MWCNTs-OH	MWCNTs-OH-5
11	[C4mim]CH_2-C_6H_4-HSO_3/MWCNTs-COOH	MWCNTs-COOH-1
12	[C4mim]CH_2-HSO_3/MWCNTs-COOH	MWCNTs-COOH-2
13	[C4mim]HSO_4/MWCNTs-COOH	MWCNTs-COOH-3
14	[C4mim]OH/MWCNTs-COOH	MWCNTs-COOH-4
15	[C4mim]Ac/MWCNTs-COOH	MWCNTs-COOH-5

Table 2. Effect of IL Amount Immobilized on MWCNTs

	amount of IL added/g				
	0.1	0.3	0.5	1	2
$m_{(MWCNTs)}$/g	0.4997	0.5000	0.5005	0.5003	0.5001
$m_{(MWCNTs-1)}$/g	0.5778	0.7641	1.2379	1.2401	1.2365
$m_{(MWCNTs-2)}$/g	0.5674	0.8037	1.0977	1.1132	1.1265
$m_{(MWCNTs-3)}$/g	0.5813	0.7928	1.2783	1.2788	1.2791
$m_{(MWCNTs\ -4)}$/g	0.5109	0.5369	0.9828	0.9941	1.0179
$m_{(MWCNTs-5)}$/g	0.5965	0.8014	1.3768	1.3805	1.3849
$m_{(MWCNTs-OH)}$/g	0.5005	0.5001	0.5000	0.5003	0.5002
$m_{(MWCNTs-OH-1)}$/g	0.6503	0.8796	1.4671	1.4665	1.4595
$m_{(MWCNTs-OH-2)}$/g	0.5928	0.7885	1.4601	1.4603	1.4589
$m_{(MWCNTs-OH-3)}$/g	0.6182	0.8524	1.4490	1.4483	1.4387
$m_{(MWCNTs-OH-4)}$/g	0.5241	0.5446	0.8597	0.8576	0.8610
$m_{(MWCNTs-OH-5)}$/g	0.6031	0.8307	1.5707	1.5719	1.5703
$m_{(MWCNTs-COOH)}$/g	0.4999	0.5000	0.4997	0.5005	0.5001
$m_{(MWCNTs-COOH1)}$/g	0.5984	0.7980	1.4798	1.4796	1.4855
$m_{(MWCNTs-COOH2)}$/g	0.6041	0.7834	1.4685	1.4785	1.4798
$m_{(MWCNTs-COOH3)}$/g	0.6097	0.7786	1.2951	1.3068	1.2997
$m_{(MWCNTs-COOH4)}$/g	0.5563	0.5707	0.9578	0.9140	0.9382
$m_{(MWCNTs-COOH5)}$/g	0.6532	0.7489	1.4724	1.4730	1.4801

Table 3. Surface Functional Group Content of MWCNT-Immobilized ILs

	content (mmol/g)			
samples	phenolic hydroxyl	carboxyl	lactone base	total acid functional group content
MWCNTs-1	0.038	0.059	0.048	0.145
MWCNTs-2	0.041	0.072	0.059	0.172
MWCNTs-3	0.043	0.079	0.068	0.190
MWCNTs-4	0.031	0.063	0.045	0.139
MWCNTs-5	0.021	0.055	0.044	0.120
MWCNTs-OH-1	0.040	0.072	0.050	0.162
MWCNTs-OH-2	0.045	0.082	0.061	0.188
MWCNTs-OH-3	0.070	0.096	0.074	0.240
MWCNTs-OH-4	0.037	0.065	0.047	0.149
MWCNTs-OH-5	0.034	0.062	0.043	0.139
MWCNTs-COOH-1	0.044	0.088	0.051	0.183
MWCNTs-COOH-2	0.048	0.091	0.063	0.202
MWCNTs-COOH-3	0.079	0.117	0.077	0.273
MWCNTs-COOH-4	0.040	0.070	0.048	0.158
MWCNTs-COOH-5	0.039	0.069	0.042	0.150

2.2. Characterization of IL Adsorbents Supported by MWCNTs. *2.2.1. Boehm Titration Analysis.* Table 3 lists the surface functional group contents of the carbon nanotube-immobilized ILs. The amount of acidic functional groups depended on the surface oxygen functional groups. The amount of acidic functional groups was highest for MWCNT-immobilized [C4mim]HSO_4. The lactone group content did not change much because lactone groups are formed via the reaction between carboxyl groups and hydroxyl groups, it is hard to generate in this process.

2.2.2. FT-IR Analysis. Figure 1 shows IR spectra of the ILs before and after immobilization on carbon nanotubes. Figure 1a shows that the spectra of [C4mim]$CH_2C_6H_4$-HSO_3, [C4mim]CH_2-HSO_3, and [C4mim]HSO_4 at 1190 cm^{-1} had characteristic peaks of R-SO_3^-- and at 1640 cm^{-1} had C═C stretching vibration frequencies. The absorption peaks near 3200 cm^{-1} correspond to C−H in the imidazole ring. Figure 1b−d shows the IR spectra of the MWCNTs with and without immobilized ILs. MWCNTs-1, MWCNTs-2, and MWCNTs-3 at 1190 cm^{-1} had characteristic peaks of R-SO_3^--, and at 1572 cm^{-1} of C−N were observed, which may be caused by the vibration of the imidazole ring. These results indicate that the ILs were successfully immobilized on the MWCNTs.

2.2.3. XPS Analysis. The XP spectra and C 1s peak splits of the MWCNT-immobilized ILs were analyzed. Figure 2 shows binding energies in the ranges corresponding to each element (O, N, C, and S). The highest-intensity binding energy at 285

https://dx.doi.org/10.1021/acsomega.0c02016
ACS Omega 2020, 5, 22827−22839

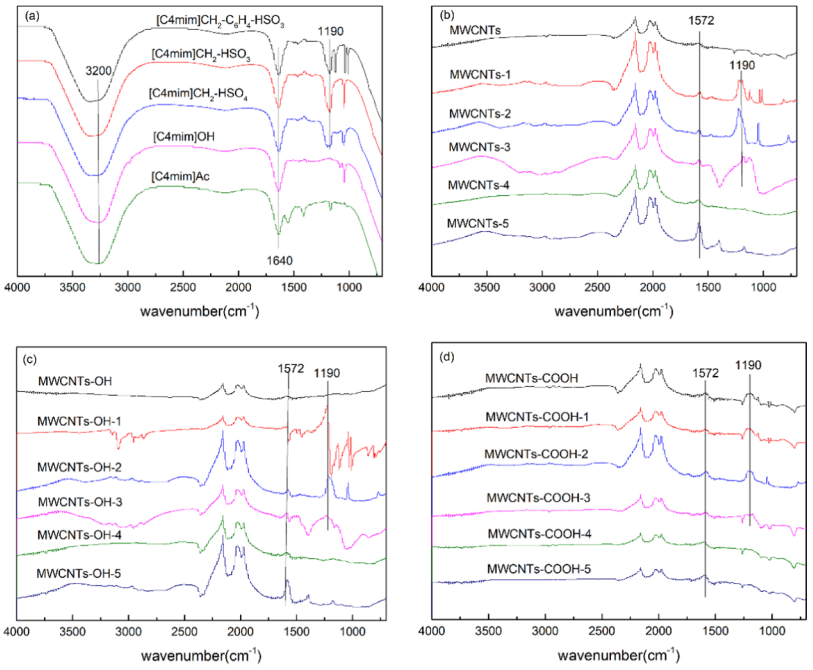

Figure 1. FT-IR spectra of ILs (a), MWCNT-immobilized ILs (b), MWCNTs-OH-immobilized ILs (c), and MWCNTs-COOH-immobilized ILs (d).

eV corresponds to C. The peaks observed at around 531.1 and 402.0 eV correspond to O and N, respectively. The intensities of the O peaks in the spectra of the samples with immobilized ILs are higher. The peak at 168.0 eV arises from [C4mim]-$CH_2C_6H_4$-HSO_3, [C4mim]CH_2-HSO_3, and [C4mim]HSO_4. The C 1s peak split spectra were analyzed. The peaks at 285.90 and 287.77 eV are attributed to C═N and C−N, respectively. The binding energy of 284.1 eV corresponds to sp^3-hybridized C−C. The presence of a peak from sp^2-hybridized C═C at 284.2 eV indicates that the MWCNTs have a graphitized structure. The S, N, C, and O contents of the MWCNT-immobilized ILs are shown in Table 4. The O contents of the immobilized IL samples were clearly higher. There was no N on the MWCNT surfaces and the N identified in the analysis was derived from imidazole in the ILs. As shown in Figures 2, S1, and S2, and Table 4, the N content on the surface of the polyhydroxy carbon nanotubes was much higher than that on the MWCNTs. This may be because of the lone pair of electrons on the Π in the imidazole ring, which would reduce the electron cloud density around N. This would facilitate electron loss and lead to Brønsted acid properties. ILs, therefore, tend to form chemical bonds with hydroxyl groups when in contact with polyhydroxy nanotubes, as well as intermolecular forces. These results indicate that the ILs were successfully immobilized on the MWCNTs.

The XP spectra and C 1s peak splits of the MWCNTs-OH and MWCNTs-COOH are shown in Figures S1 and S2.

2.2.4. BET Analysis. The pore structures of the MWCNTs with immobilized ILs were investigated by performing BET analysis; the results are shown in Figure 3. The figure shows that the N_2 adsorption isotherms were type IV, as defined by the International Union of Pure and Applied Chemistry. The figure shows no clear adsorption in the low-pressure area. The curve in the high-pressure area shows a clear upward trend, which indicates a microporous structure, with few micropores. The hysteresis loop in the region P/P_0 = 0.8−1.0, which can be regarded as an H1-type hysteresis loop, indicates a material with evenly distributed pores and interconnected channels. The structural characteristics of the MWCNTs and activated carbon (AC) before and after immobilization ILs are shown in Table 5. The surface areas of the adsorbents with immobilized ILs decreased to different degrees and the adsorption average pore width increased. This may be because the IL entered the MWCNT channels or the MWCNT surface collapsed. In addition, the specific surface area of AC was larger than MWCNTs, which may be due to the activation and porous surface of AC, so its adsorption capacity is better than MWCNTs. The N_2 adsorption−desorption isotherms of the other samples are shown in Figures S3−S6.

2.2.5. TG-DTG Analysis. Figure 4 shows the TG-DTG curves for the samples. The TG data show that the first weight loss occurred at temperatures below 100 °C, and probably represents water evaporation. At 250−400 °C, the samples with immobilized [C4mim]$CH_2C_6H_4$-HSO_3, [C4mim]CH_2-HSO_3, and [C4mim]HSO_4 showed high weight losses, as a result of IL decomposition. The DTG curves show that these three ILs showed slight weight losses at 100−250 °C. At this stage, the samples absorbed heat slowly, the rate of weight loss was low, and there was little change in the sample quality. In the pyrolysis stage, i.e., 250−400 °C, the samples decomposed violently, and the highest decomposition rate was observed at 400 °C. Thermal decomposition basically ends above 400 °C. Compared with the thermal stabilities of the samples with these ILs, the thermal stabilities of the samples with immobilized [C4mim]OH and [C4mim]Ac were poor. This may be because the two basic ILs have poor thermal stabilities and low adsorption rates. On the basis of the thermogravimetric data, acidic ILs were selected for subsequent experiments.

2.3. Single-Factor Analysis of Cr(VI) Adsorption by MWCNTs-ILs. *2.3.1. Effect of Adsorbent.* The effects of the adsorbent dosage on the Cr(VI) removal rate and equilibrium adsorption capacity in aqueous solution are shown in Figure 5. The Cr(VI) removal rate increased, and the equilibrium

https://dx.doi.org/10.1021/acsomega.0c02016
ACS Omega 2020, 5, 22827−22839

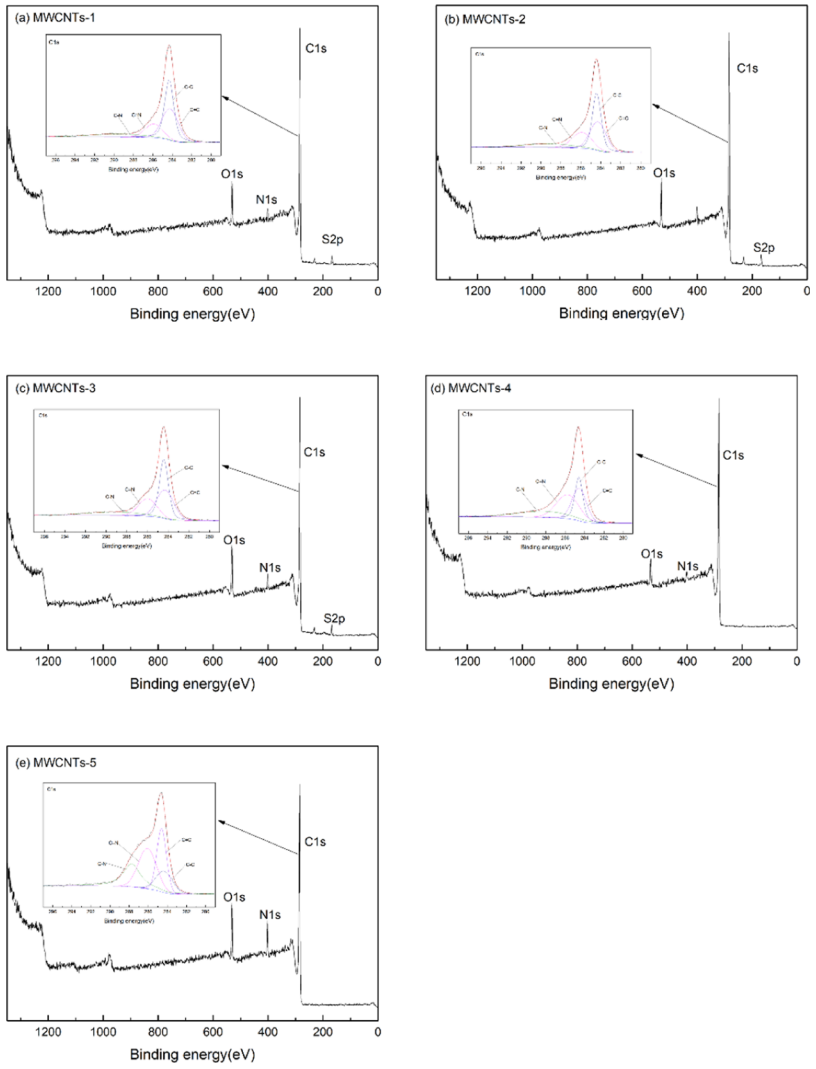

Figure 2. XP spectra of MWCNTs-1 and C 1s peak split spectra (a), MWCNTs-2 and C 1s peak split spectra (b), MWCNTs-3 and C 1s peak split spectra (c), MWCNTs-4 and C 1s peak split spectra (d), and MWCNTs-5 and C 1s peak split spectra (e).

Table 4. Element (S, N, C, and O) Content of MWCNT-Immobilized ILs

samples	$At._{S\ 2p}$ (%)	$At._{N\ 1s}$ (%)	$At._{C\ 1s}$ (%)	$At._{O\ 1s}$ (%)
MWCNTs	0.22	1.87	95.14	2.76
MWCNTs-1	1.63	3.34	88.78	6.26
MWCNTs-2	2.19	3.37	87.36	7.09
MWCNTs-3	2.09	4.62	84.52	8.77
MWCNTs-4	0.24	0.77	90.69	5.29
MWCNTs-5	0.26	7.08	84.74	7.92
MWCNTs-OH	0.21	2.76	93.74	3.29
MWCNTs-OH-1	1.54	3.77	84.87	9.82
MWCNTs-OH-2	1.88	3.47	85.91	8.73
MWCNTs-OH-3	3.05	5.55	77.87	13.53
MWCNTs-OH-4	0.28	3.67	91.61	4.44
MWCNTs-OH-5	0.26	3.27	92.6	3.87
MWCNTs-COOH	1.21	3.33	82.06	13.4
MWCNTs-COOH-1	3.58	5.59	73.88	16.95
MWCNTs-COOH-2	4.71	7.73	69.95	17.62
MWCNTs-COOH-3	4.49	7.91	68.39	19.22
MWCNTs-COOH-4	0.25	4.36	89.21	6.18
MWCNTs-COOH-5	0.31	4.68	82.22	12.78

adsorption capacity decreased, with increasing amount of the adsorbent. When the amount of the adsorbent was less than 50.0 mg, Cr(VI) adsorption accelerated and the removal rate increased. When the amount of the adsorbent exceeded 50.0 mg, the Cr(VI) removal rate was basically constant. The amount of oxygen-containing groups on the MWCNTs increased, which promoted Cr(VI) adsorption. When the Cr(VI) concentration was constant, the amount adsorbed increased, the equilibrium concentration of the solution decreased, and the adsorption force decreased. On the basis of these experimental results, an adsorbent dosage of 50.0 mg was selected for subsequent experiments.

2.3.2. Effect of Adsorption Temperature. The effect of temperature on Cr(VI) adsorption by MWCNTs was investigated; the results are shown in Figure 6. The Cr(VI) removal rate by the adsorbent did not significantly change as the temperature was increased from 20 to 40 °C. At temperature above 40 °C, the Cr(VI) removal rate by the adsorbent decreased, probably because desorption of Cr(VI) from the nanotube surfaces occurred at higher temperatures. The increased amounts of oxygen functional groups on the MWCNT surfaces promoted Cr(VI) adsorption. The Cr(VI) removal rates at 40 °C were 43.19% (MWCNTs), 44.00%

https://dx.doi.org/10.1021/acsomega.0c02016
ACS Omega 2020, 5, 22827−22839

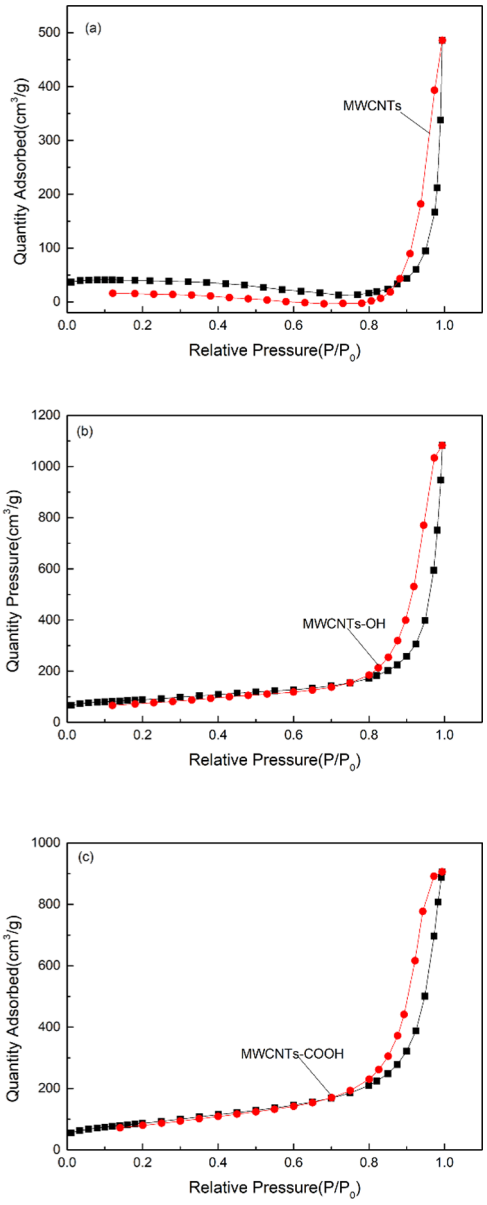

Figure 3. N_2 adsorption−desorption isotherms curves for MWCNTs (a), MWCNTs-OH (b), and MWCNTs-COOH (c).

(MWCNTs-OH), and 46.05% (MWCNTs-COOH). The optimum adsorption temperature was, therefore, 40 °C.

2.3.3. Effect of pH. Figure 7 shows the effect of pH on Cr(VI) adsorption by the MWCNTs. The figure shows that the Cr(VI) removal rate by the adsorbent decreased with increasing pH. Under acidic conditions, the Cr(VI) removal rates of MWCNTs-3, MWCNTs-OH-3, and MWCNTs-COOH reached 38.42, 40.81, and 44.14%, respectively. The reason is that at pH 2.0−6.0, CrO_2^{4-} reacts with H^+ to form $Cr_2O_2^{7-}$. Under strongly acidic conditions, Cr(VI) can exist in various forms, e.g., $Cr_2O_2^{7-}$, $HCrO^{4-}$, $Cr_3O_2^{10-}$, and $Cr_4O_2^{13-}$.[34] At a pH greater than 8.0, Cr(VI) can only exist in water as CrO_2^{4-}. Under acidic conditions, the adsorbent surface is highly protonated, and the adsorbent more easily adsorbs anionic forms of Cr(VI) polymers. Protonation decreases with increasing pH, electrostatic interactions between the adsorbent and adsorbate decrease continuously, the concentration of OH^- increases, and there is competitive adsorption with CrO_2^{4-}. The Cr(VI) removal therefore decreases. The optimum experimental pH is, therefore, 2.0.

2.3.4. Effect of Cr(VI) Initial Concentration. Figure 8 shows that as the initial concentration of Cr(VI) increased, the adsorption capacity of the adsorbent increased gradually, but the Cr(VI) removal rate decreased. This is because as the Cr(VI) concentration increases, adsorption between the adsorbent and chromium moved from the boundary of the chromium solution to the surface of the adsorbent. In the initial stage, Cr(VI) species occupied active adsorption sites, and the adsorption capacity increased. However, the number of active adsorption sites on the adsorbent is limited. The Cr(VI) removal rate decreased gradually with increasing Cr(VI) concentration. When the Cr(VI) concentration was 60 mg/L, the removal rates of MWCNTs-3, MWCNTs-OH-3, and MWCNTs-COOH-3 reached 34.68, 37.06, and 44.24%, and the adsorption capacities reached 20.81, 22.34, and 24.14 mg/L, respectively. These results show that the optimum Cr(VI) concentration was 60.00 mg/L.

2.3.5. Effect of Adsorption Time. Figure 9 shows that the adsorption rate increased rapidly for 200 min and the Cr(VI) removal rate also increased. Then, the removal rate slowed down. This is because the number of adsorption sites on the MWCNTs was limited. As adsorption progressed, most adsorption sites became occupied. The adsorption rate therefore slowed down, the removal rate became basically stable, and the adsorption equilibrium was reached. These results indicate that the optimum adsorption time was 200 min.

2.3.6. Comparison with Other Results. The experimental results were compared with other researchers concerning the Cr(VI) removal from a water phase; the results are shown in Table 6. The adsorption capacity of the MWCNT-ILs reached 31.29 mg/g under the optimal conditions. The experimental results were compared with that of MWCNTs, polyaniline/multiwalled carbon nanotube (MWCNTs-PANI), magnetic iron oxide nanoparticle multiwalled carbon nanotube (MWCNTs-MIO), and oxidized MWCNTs were used as adsorbents. The results show that the MWCNT-immobilized ILs exhibit better adsorption performance.

2.4. Adsorption Isothermal Model Study. The Langmuir and Freundlich models were used to fit the experimental data; the results are shown in Table 7. The correlation coefficient for the Freundlich model was slightly higher than that for the Langmuir model, i.e., the experimental adsorption results were more consistent with the Freundlich model. This indicates that Cr(VI) adsorption by MWCNTs is multilayer adsorption. The Q_{max} and k_F values increased, and R^2 decreased, with increasing temperature. This indicates that high temperatures promoted adsorption and the adsorption process was more stable at low temperatures.

The isothermal adsorption models for the MWCNTs are shown in Figure S6.

2.5. Adsorption Kinetic Model Study. A study of the adsorption kinetics was performed; the fitting results are shown in Table 8. The pseudo-first-order dynamic model is based on a single-adsorption process or mechanism in which the reaction rate is only affected by the adsorption site, and boundary resistance is the main controlling factor. The pseudo-second-order dynamic model is based on the rate-controlling step for a chemical reaction or chemical adsorption, which involves gain and loss through electron sharing. Fitting was clearly better with the pseudo-second-order kinetic model than

https://dx.doi.org/10.1021/acsomega.0c02016
ACS Omega 2020, 5, 22827−22839

Table 5. Structural Characteristics of MWCNT-Immobilized ILs

samples	BET surface area (m^2/g)	BJH adsorption cumulative volume of pores (cm^3/g)	*t*-plot micropore volume (cm^3/g)	adsorption average pore width (nm)
MWCNTs	324.7020	0.7517	0.07593	11.2855
MWCNTs-1	165.9781	1.2323	0.005886	16.9209
MWCNTs-2	169.0748	1.1376	0.01165	15.9259
MWCNTs-3	183.1114	1.2188	0.01428	15.3509
MWCNTs-4	200.5826	2.1250	0.02199	13.7451
MWCNTs-5	206.9164	1.5591	0.02050	14.8614
MWCNTs-OH	298.1032	1.6537	0.05325	12.3429
MWCNTs-OH-1	140.4670	0.3423	0.003148	16.4919
MWCNTs-OH-2	189.3151	0.4403	0.01145	17.8182
MWCNTs-OH-3	143.8319	0.3209	0.002887	17.4183
MWCNTs-OH-4	277.6813	1.6290	0.03159	15.1885
MWCNTs-OH-5	168.0445	0.5136	0.02571	16.8590
MWCNTs-COOH	310.7104	1.4134	0.06143	13.8789
MWCNTs-COOH-1	141.4255	0.1527	0.002097	18.1824
MWCNTs-COOH-2	171.8163	0.3471	0.01283	21.2774
MWCNTs-COOH-3	150.7022	0.2074	0.006316	22.4464
MWCNTs-COOH-4	204.9390	1.2125	0.02099	15.1205
MWCNTs-COOH-5	176.5221	0.7114	0.01985	18.2054
AC	1204.9595	0.1657	0.3638	2.1625
AC-1	285.5915	0.01742	0.03314	2.0004
AC-2	503.3910	0.1349	0.09650	2.1492
AC-3	821.3599	0.1586	0.2004	2.1843
AC-4	890.6183	0.1405	0.2552	2.1589
AC-5	742.5383	0.1377	0.1818	2.1943

with the pseudo-first-order kinetic model. The correlation coefficients of the pseudo-second-order kinetic model after fitting were all greater than 0.99. This indicates that the adsorption rate was related to the adsorption sites. The adsorption of Cr(VI) by the adsorbent was, therefore, more in line with the pseudo-second-order kinetic equation. This indicates that chemical adsorption was the main adsorption process.

The kinetic models for adsorption of Cr(VI) are shown in Figure S7.

2.6. Thermodynamic Analysis. The adsorption thermodynamic data are shown in Table 9. The data show that ΔH is less than 0, which indicates that the adsorption of chromium on carbon nanotubes is an exothermic reaction. The ΔS value is less than 0, which indicates that in the adsorption process, the typical entropy decreases. The adsorbents are aligned from the free motion state to the surface of the adsorbent, and the confusion decreases.

2.7. Recycling of the Immobilized IL Adsorbent. Figure 10 shows that after five cycles, the Cr(VI) removal rate by MWCNTs-3, MWCNTs-OH-3, and MWCNTs-COOH-3 decreased by 27.97, 9.39, and 7.34%, respectively. The MWCNT surfaces contain carboxyl groups. The reusability of the MWCNTs is higher than those of adsorbents with no surface hydroxyl or carboxyl groups. These results show that MWCNT-immobilized ILs have good recyclability.

2.8. Mechanism of Cr(VI) Adsorption by MWCNTs in a Water Phase. The general mechanism for Cr(VI) adsorption by MWCNTs is shown in Figure 11. MWCNT-immobilized ILs washed in deionized water may be held together by electrostatic or van der Waals forces. Imidazole ILs contain nitrogen. So in the case of polyhydroxy MWCNT-immobilized ILs, there is an ionic bond between the surface hydroxyl group and the Brønsted acid's N in addition to electrostatic adhesion and intermolecular forces. Hydrogen bonds are formed because N itself is electronegative. Although the binding energies are not measured in this study, it is certain that the binding energies between imidazoles ILs and polyhydroxyl MWCNTs are higher than those of MWCNTs. After immobilization, the contents of S, N, and O in the MWCNTs increase. This indirectly proves that various types of ILs can be successfully immobilized on MWCNTs. During Cr(VI) adsorption, the inorganic anions in the IL are replaced by Cr(VI). The Cr(VI) in water is therefore adsorbed and heavy-metal ion removal from water is achieved. The recovery of the MWCNT adsorbents in this study was good, and high adsorption capacity was retained for many cycles.

3. CONCLUSIONS

A supported IL adsorbent was synthesized by immobilizing ILs, namely, [C4mim]$CH_2C_6H_4$-HSO_3, [C4mim]CH_2-HSO_3, [C4mim]HSO_4, [C4mim]OH, and [C4mim]Ac, on MWCNTs (MWCNTs, MWCNTs-OH, and MWCNTs-COOH). The ratio of MWCNTs to [C4mim]HSO_4 was 1:1. Boehm titration results showed that IL immobilization changed the oxygen-containing functional groups on the adsorbent surface, and acidic functional groups were fixed at certain sites. The FT-IR spectra of the MWCNTs with immobilized ILs contained absorption peaks form sulfonate groups and imidazole rings. XPS showed the presence of different elements and the types of functional groups. BET analysis showed that the pore structures of the adsorbents were changed by IL immobilization, and the specific surface areas decreased to various degrees. TG-DTG showed that the adsorbents had good thermal stability.

The three types of MWCNTs (MWCNTs, MWCNTs-OH, and MWCNTs-COOH) with immobilized ILs were used to remove Cr(VI) from an aqueous solution. The results show

https://dx.doi.org/10.1021/acsomega.0c02016
ACS Omega 2020, 5, 22827−22839

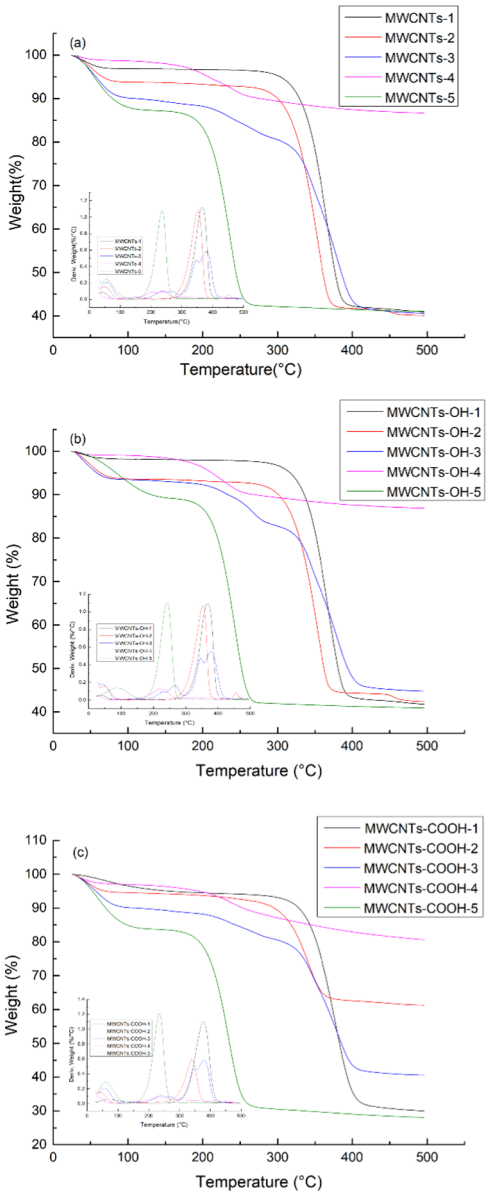

Figure 4. TG and DTG curves for MWCNT-immobilized ILs (a), MWCNTs-OH-immobilized ILs (b), and MWCNTs-COOH-immobilized ILs (c).

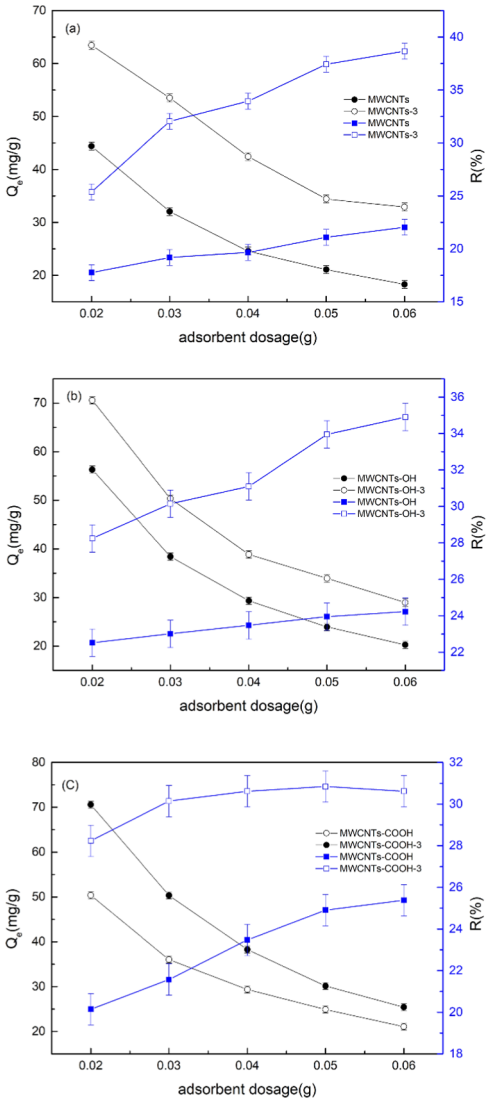

Figure 5. Effect of adsorbent dosage on Cr(VI) adsorption by MWCNT-immobilized ILs (a), MWCNTs-OH-immobilized ILs (b), and MWCNTs-COOH-immobilized ILs (c).

that under the conditions with the initial concentration Cr(VI) 60.00 mg/L, MWCNT dosage 50.0 mg, pH 2.0, adsorption temperature 40 °C, and adsorption time 200 min, the adsorption capacities were 26.00 mg/g (MWCNTs), 28.43 mg/g (MWCNTs-OH), and 31.29 mg/g (MWCNTs-COOH), and the Cr(VI) removal rates reached 43.33% (MWCNTs), 47.38% (MWCNTs-OH), and 52.14% (MWCNTs-COOH). It was obvious that the adsorption capacity and the Cr removal rate by MWCNTs-COOH were higher. This further supports the XPS and BET results. Polyhydroxy MWCNT-immobilized ILs have more capacity to hold ILs due to chemical bonding. Moreover, after the ILs were immobilized, the polyhydroxyl MWCNTs could play a role of pH self-regulation in the solution, which was more conducive to adsorption. During the experiment, the adsorption capacity of AC-immobilized ILs was also studied. The adsorption capacity of AC-IL on chromium reached 76.04 mg/g. The results showed that the adsorption capacity of AC-IL was better than MWCNTs-IL. However, a large amount of NaOH was used for AC activation, which caused environmental pollution and complicated follow-up treatment. Therefore, the research for Cr(VI) adsorption on MWCNTs-IL was necessary. The adsorption isotherm fitting showed that the process conformed to the Freundlich model. This indicates that the adsorption process was in line with the multilayer adsorption theory. The ability to adsorb Cr(VI) fitted the pseudo-second-order dynamic model. This indicates that the adsorption process was mainly chemical adsorption. Thermodynamic analysis showed that the adsorption process is endothermic. After five cycles, the Cr(VI) removal rate by MWCNTs-3, MWCNTs-OH-3, and MWCNTs-COOH-3 decreased by 27.97, 9.39, and 7.34%, respectively.

4. MATERIALS AND METHODS

4.1. Materials and Reagents. *4.1.1. Materials.* MWCNTs, MWCNTs-OH, and MWCNTs-COOH were purchased from the Chinese Academy of Sciences Chengdu Organic Chemistry Co., Ltd. (Chengdu, China).

https://dx.doi.org/10.1021/acsomega.0c02016
ACS Omega 2020, 5, 22827−22839

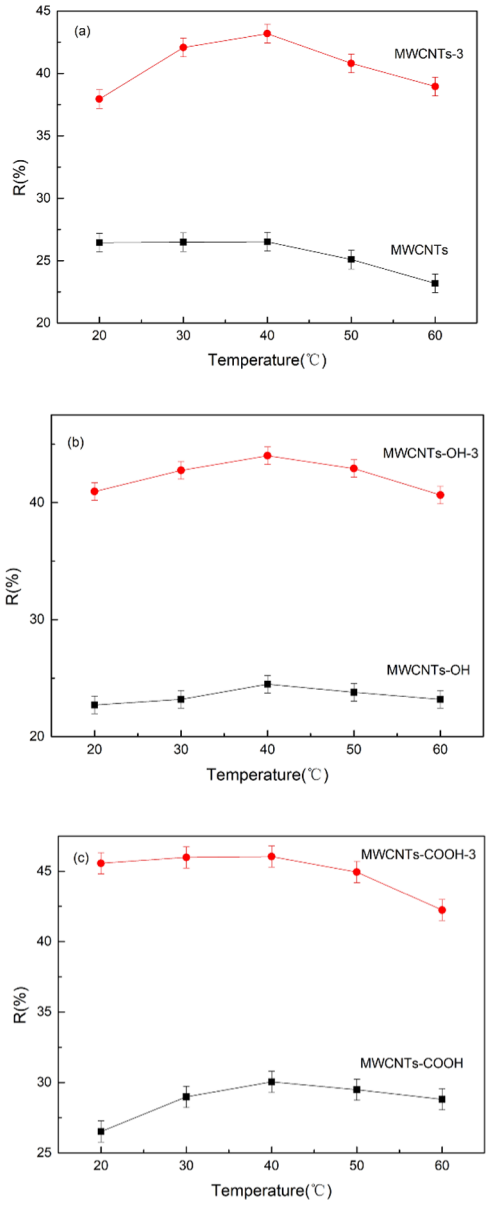

Figure 6. Effect of temperature on Cr(VI) adsorption by MWCNT-immobilized ILs (a), MWCNTs-OH-immobilized ILs (b), and MWCNTs-COOH-immobilized ILs (c).

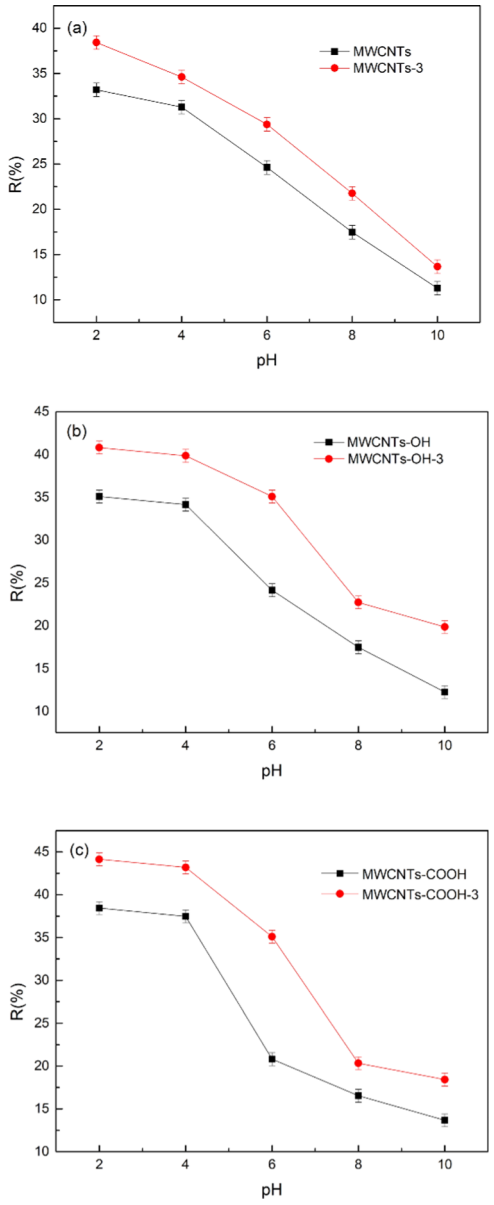

Figure 7. Effect of pH on Cr(VI) adsorption by MWCNT-immobilized ILs (a), MWCNTs-OH-immobilized ILs (b), and MWCNTs-COOH-immobilized ILs (c).

4.1.2. Chemical Reagents. The ILs, namely, [C4mim]-$CH_2C_6H_4$-HSO_3, [C4mim]CH_2-HSO_3, [C4mim]HSO_4, [C4mim]OH, and [C4mim]Ac, used in this work were purchased from Cheng Jie Chemical Co., Ltd. (Shanghai, China). Methyl red, phenolphthalein, phosphoric acid, and acetone were purchased from Tianjin Kemiou Chemical Reagent Co., Ltd. (Tianjin, China). Sodium hydroxide and potassium dichromate were purchased from Guangfu Chemical Reagents Co. (Tianjin, China). Deionized water was obtained using a Milli-Q Water Purification System (Millipore, MA). Hydrochloric acid and concentrated sulfuric acid were purchased from Beijing Chemical Plant. Diphenylcarbonyl hydrazine was purchased from Maclean Biochemical Technology Co., Ltd. (Shanghai, China).

4.2. Methods. *4.2.1. Preparation of the Immobilized IL Catalyst.* As shown in Figure 12a, MWCNTs, MWCNTs-OH, or MWCNTs-COOH (0.50 g) were, respectively, added to five different conical flasks. Five types of IL were then, respectively, added to the conical flasks. Ethanol had to be removed from [C4mim]OH by distillation before [C4mim]OH was used. Deionized water (50 mL) was added to the mixed solutions in the conical flasks. The flasks were shaken in a water bath at room temperature. After 24 h, the products were removed by filtration, washed, and dried at 110 °C. The electronegative N in the imidazole group in the ILs forms hydrogen bonds with hydroxide ions on MWCNTs; this enables IL immobilization on MWCNTs. Activated carbon (AC) was pretreated with nitric acid and AC-immobilized ILs by the same method as above.

4.2.2. Characterization of Carbon Material-Immobilized IL Adsorbents. The acid−base properties and surface acidic functional groups of the MWCNTs were investigated by Boehm titration. Fifty milliliters of NaOH, Na_2CO_3, and $NaHCO_3$ (0.10 mol/L) were added to MWCNT-immobilized

https://dx.doi.org/10.1021/acsomega.0c02016
ACS Omega 2020, 5, 22827−22839

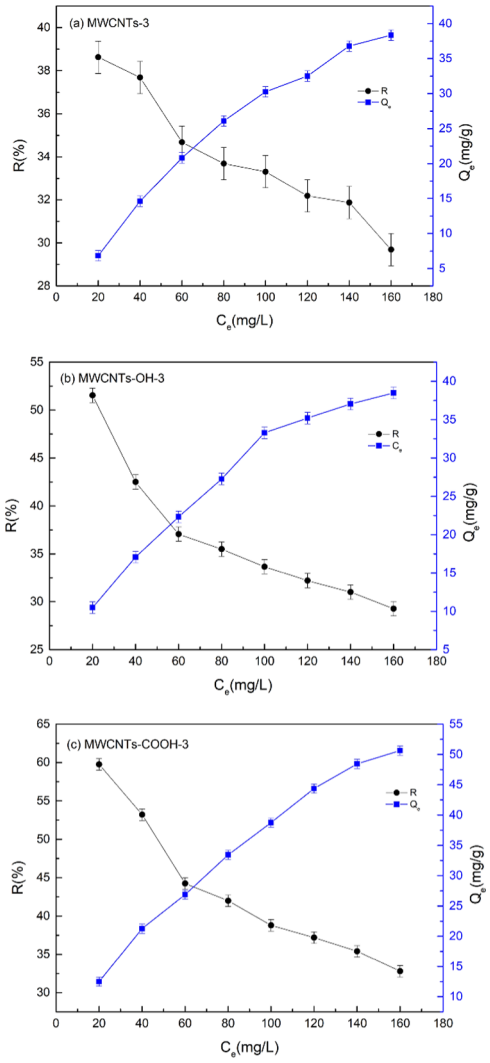

Figure 8. Effect of Cr(VI) initial concentration on Cr(VI) adsorption by MWCNT-immobilized ILs (a), MWCNTs-OH-immobilized ILs (b), and MWCNTs-COOH-immobilized ILs (c).

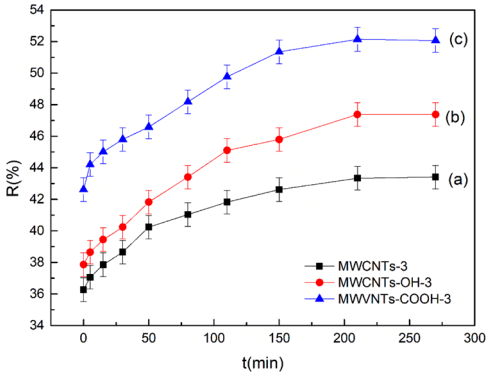

Figure 9. Effect of adsorption time on MWCNT-immobilized ILs (a), MWCNTs-OH-immobilized ILs (b), and MWCNTs-COOH-immobilized ILs (c).

ILs, and the mixture was titrated with HCl (0.10 mol/L). The acidic functional group content n (mmol/g) in the reaction per unit mass of MWCNTs with standard lye was calculated according to eqs 1−9.[39,40]

Table 6. Comparison with Other Researchers Concerning the Removal of Cr(VI)

number	adsorbent	Q_e (mg/g)	refs
1	MWCNTs	24.00	35
2	MWCNTs-PNAI	28.25	36
3	MWCNTs-MIO	11.256	37
4	Oxidized MWCNTs	4.2615	38
5	MWCNTs-ILs	31.29	

$$n_{NaOH} = [C_{NaOH}V_{NaOH} - c_{HCl}(V_{HCl} - \Delta V_1 - V_b)]/W \quad (1)$$

$$n_{Na_2CO_3} = [2c_{Na_2CO_3}V_{Na_2CO_3} - c_{HCl}(V_{HCl} - \Delta V_2 - V_b)]/W \quad (2)$$

$$n_{NaHCO_3} = [c_{NaHCO_3}V_{NaHCO_3} - c_{HCl}(V_{HCl} - \Delta V_3 - V_b)]/W \quad (3)$$

$$\Delta V_1 = (V_{NaOH} + V_{HCl})([H^+]^R - [H^+]^{T_1})/c_{HCl} \quad (4)$$

$$\Delta V_2 = (2V_{Na_2CO_3} + V_{HCl})([H^+]^R - [H^+]^{T_2})/c_{HCl} \quad (5)$$

$$\Delta V_3 = (V_{NaHCO_3} + V_{HCl})([H^+]^R - [H^+]^{T_3})/c_{HCl} \quad (6)$$

$$n_{RCOOH} = n_{NaHCO_3} \quad (7)$$

$$n_{RCOOCOR'} = n_{Na_2CO_3} - n_{NaHCO_3} \quad (8)$$

$$n_{ArOH} = n_{NaOH} - n_{Na_2CO_3} \quad (9)$$

where W (g) is the sample dosage, V_b (mL) is the distilled water blank volume, V_{HCl} (mL) is the volume of the standard solution consumed by HCl, c_i (mol/L) is the concentration of the standard solution, ΔV (mL) is the change in the volume of the HCl standard solution at the end point of the acid−base titration, $[H^+]^R$ ($=10^{-5}$ mol/L) is the theoretical proton concentration of methyl red, which indicates the end point, and $[H^+]^{T1}$, $[H^+]^{T2}$, and $[H^+]^{T3}$ are the proton concentrations at the theoretical end points when HCl was titrated with NaOH, Na_2CO_3, and $NaHCO_3$, respectively.

FT-IR spectra of the samples were recorded with an IS10 FT-IR spectrometer (Nicolet). The sample was placed on an attenuated total reflectance attachment and spectra were recorded in the range of 4000−400 cm^{-1} at a resolution of 4 cm^{-1}.

XPS was used (PHI5700 spectrometer, Micromeritics Company) to identify the states of chemical functional groups and elements on the sample surfaces.

The BET method was used to calculate the specific surface areas (ASAP2020 specific surface area analyzer, Micromeritics Company) and N_2 adsorption−desorption curves were recorded.

The thermal stabilities of the samples were determined with a Q50 thermogravimetric analyzer (American TA Company); the N_2 flow rate was 30 mL/min and the temperature was raised at 10 °C/min for N_2 adsorption−desorption.

4.2.3. Preparation of MWCNTs-ILs. First step: Potassium dichromate (0.2942 ± 0.0001 g) was dried at 110 °C for 2 h, added to a conical flask, and dissolved in deionized water in a 1000 mL flask to obtain a chromium standard reserve solution of concentration 1×10^{-3} mol/L. The chromium standard reserve solution (1.0 mL) was placed in a 100 mL flask to obtain a solution of concentration 1×10^{-5} mol/L. Diphenylcarbonyl hydrazine (DPCI) (0.1211 ± 0.0001 g)

https://dx.doi.org/10.1021/acsomega.0c02016
ACS Omega 2020, 5, 22827−22839

Table 7. Isothermal Model Parameters of Cr(VI) Adsorption at Different Temperatures

		Langmuir model		Freundlich model			
	t (°C)	k_L (L/mg)	Q_{max} (mg/g)	R^2	k_F	n	R^2
MWCNTs-3	25	0.005090	98.8376 ± 0.75%	0.9818	0.8861	1.2678	0.9983
	40	0.009337	80.5809 ± 0.75%	0.9951	1.5983	1.4314	0.9992
	55	0.007676	104.5007 ± 0.75%	0.9971	1.6444	1.3740	0.9994
MWCNTs-OH-3	25	0.009491	73.5304 ± 0.75%	0.9883	1.4511	1.4261	0.9956
	40	0.008665	94.9668 ± 0.75%	0.9911	1.6916	1.3994	0.9985
	55	0.009813	102.0408 ± 0.75%	0.9915	2.0676	1.4205	0.9988
MWCNTs-COOH-3	25	0.01012	91.9118 ± 0.75%	0.9783	2.2371	1.5154	0.9974
	40	0.01494	86.9565 ± 0.75%	0.9900	3.5339	1.6949	0.9986
	55	0.01391	107.5269 ± 0.75%	0.9884	3.7577	1.6139	0.9984

Table 8. Pseudo-Primary and Pseudo-Second-Order Kinetic Model Fitting Parameters of Cr(VI) Adsorption

	quasi-first-order dynamic model			quasi-second-order dynamic model		
adsorbent	k_1 (min^{-1})	R^2	Q_e (mg/g)	k^2 (g/(mg min))	R^2	Q_e (mg/g)
MWCNTs-3	0.01078	0.9938	2.2897 ± 0.75%	0.01378	0.9999	26.1780 ± 0.75%
MWCNTs-OH-3	0.00961	0.9904	2.6154 ± 0.75%	0.008095	0.9997	28.7356 ± 0.75%
MWCNTs-COOH-3	0.00894	0.8592	2.3573 ± 0.75%	0.009111	0.9996	31.5457 ± 0.75%

Table 9. Thermodynamic Parameters for Cr(VI) Adsorption onto MWCNTs

	T (K)	ΔG (kJ/mol)	ΔH (J/mol)	ΔS [J/(mol/K)]
MWCNTs-3	298	10.4051	−14.5537	−45.8891
	313	3.0119		
	328	1.9056		
MWCNTs-OH-3	298	7.1904	−10.1306	−33.3333
	313	3.5115		
	328	1.2686		
MWCNTs-COOH-3	298	3.7401	−3.2641	−15.3052
	313	2.4284		
	328	1.9754		

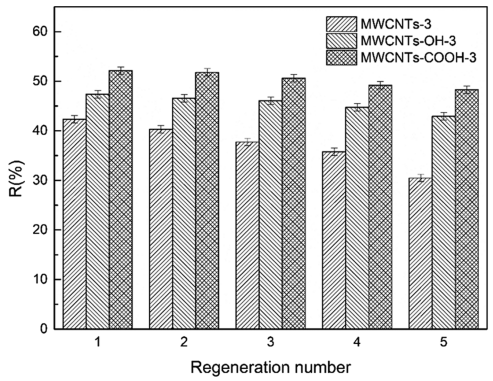

Figure 10. Reuse of MWCNT-immobilized ILs.

was added to a 50 mL beaker and dissolved in acetone. The solution was put in a 100 mL flask and used immediately.

Second step: The chromium standard reserve solution (0.0, 0.2, 0.5, 1.0, 2.0, 4.0, or 6.0 mL) was added to a 50 mL colorimetric tube, and water was added to the mark. (1 + 1) H_2SO_4 (0.50 mL), (1 + 1) H_3PO_4 (0.5 mL), and DPCI (1 mL) were added to the solution and uniformly mixed. The reagent solution (i.e., a solution without chromium) was used as a reference; the UV absorbance was measured at 540 nm, and a standard curve for chromium was constructed: $Y = 0.0021X + 0.0007$ ($R^2 = 0.9990$), where Y is the absorbance (A) and X is the solution concentration (C_e). The equilibrium adsorption capacity of the sample (Q_e) and the Cr(VI) removal rate (R) were calculated from eqs 10 and 11, respectively.

$$Q_e = \frac{V(C_0 - C_e)}{m} \tag{10}$$

$$R(\%) = \frac{C_0 - C_e}{C_0} \times 100 \tag{11}$$

Third step: As shown in Figure 12b, a solution of a certain concentration of chromium and MWCNTs-3, MWCNTs-OH-3, or MWCNTs-COOH-3 (50.0 mg) was added; the initial solution pH was adjusted to 2 with HNO_3. The mixtures were shaken for a certain time at 150 r/min at 40 °C. After adsorption equilibrium was reached, the solution was filtered with a 0.22 μm filter membrane and the UV absorbance was measured. Adsorption tends to equilibrium, therefore the Langmuir model (eq 12) and Freundlich model (eq 13) were used to clarify the surface properties of the adsorbents and the interactions between adsorbents and adsorbates. The Langmuir model assumes that the adsorbent is adsorbed on a single surface by single-molecular-layer adsorption and there is no interaction between the adsorbent and adsorbed molecule. The Freundlich model describes multilayer adsorption, in which the adsorption capacity continues to increase with increasing concentration. The adsorption time and capacity were studied by investigating the kinetics of Cr(VI) adsorption. A first-order kinetic equation (eq 14) and second-order kinetic equation (eq 15) were used to fit the experimental results. The Gibbs free-energy change (ΔG, kJ/mol) enthalpy change (ΔH, kJ/mol), and entropy change [ΔS, J/(mol/K)] were calculated using the Van't Hoff equation (eqs 16 and 17).

$$\frac{C_e}{Q_e} = \frac{C_e}{Q_{max}} + \frac{1}{Q_{max} k_L} \tag{12}$$

$$\ln Q_e = \ln k_F + \frac{1}{n} \ln C_e \tag{13}$$

$$\ln(Q_e - Q_t) = \ln Q_e - k_1 t \tag{14}$$

https://dx.doi.org/10.1021/acsomega.0c02016
ACS Omega 2020, 5, 22827−22839

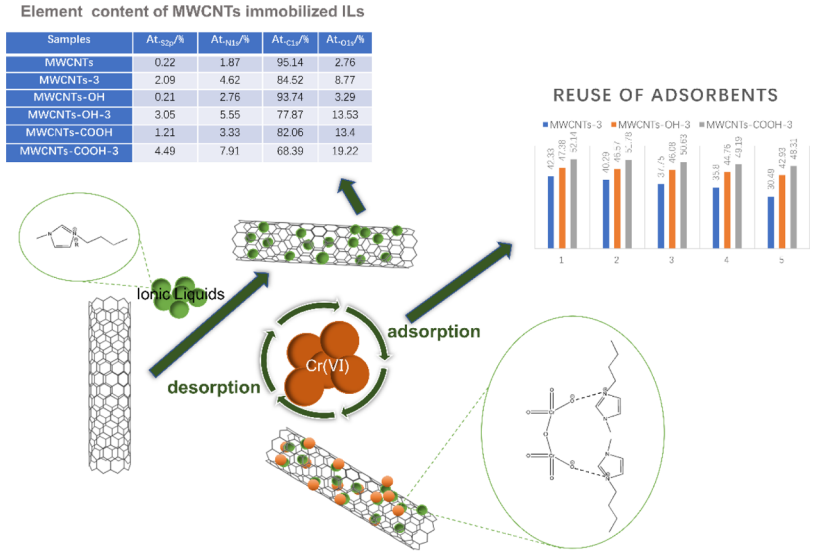

Figure 11. Adsorption mechanism diagram of Cr(VI) by MWCNT-immobilized ILs from a water phase.

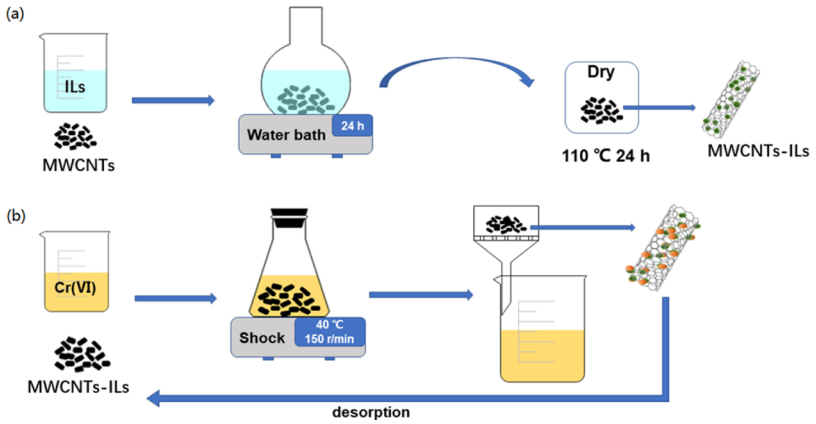

Figure 12. Preparation of MWCNTs-ILs.

$$\frac{t}{Q_t} = \frac{1}{k_2 Q_e^2} + \frac{t}{Q_e} \quad (15)$$

$$\Delta G = -RT\ln K \quad (16)$$

$$\ln K = -\frac{\Delta H}{RT} + \frac{\Delta S}{R} \quad (17)$$

In the equations, C_e (mg/L) is the concentration of Cr(VI) in the solution after adsorption equilibrium, Q_e (mg/g) is the equilibrium adsorption rate, Q_{max} (mg/g) is the maximum amount adsorbed by the adsorbent, k_L (L/mg) is the Langmuir equilibrium adsorption constant, k_F and n are the Freundlich adsorption empirical constants, Q_t (mg/g) is the adsorption capacity at time t, k_1 (1/min) is the first-order kinetic rate constant, k_2 [g/(mg min)] is the second-order kinetic rate constant, R is the universal gas constant (8.314 J/mol/K), T is the temperature (K), and K is the equilibrium constant.

■ ASSOCIATED CONTENT

Supporting Information

The Supporting Information is available free of charge at https://pubs.acs.org/doi/10.1021/acsomega.0c02016.

XPS spectra of MWCNTs-OH-immobilized ILs and C 1s peak split spectra (Figure S1); XPS spectra of MWCNTs-COOH-immobilized ILs and C 1s peak split spectra (Figure S2); N_2 adsorption−desorption isotherms curves of MWCNT-immobilized ILs (Figure S3); N_2 adsorption−desorption isotherms curves of MWCNTs-OH-immobilized ILs (Figure S4); N_2 adsorption−desorption isotherms curves of MWCNTs-COOH-immobilized ILs (Figure S5); N_2 adsorption−desorption isotherms curves of AC-immobilized ILs (Figure S6); adsorption isothermal curves of MWCNTs-3, MWCNTs-OH-3, and MWCNTs-COOH-3 (Figure S7); pseudo-kinetic model for adsorption of Cr(VI) by MWCNT-immobilized ILs (Figure S8) (PDF)

■ AUTHOR INFORMATION

Corresponding Authors

Chunhui Ma − *Key Laboratory of Bio-based Material Science and Technology (Ministry of Education), College of Material Science and Engineering, Northeast Forestry University, 150040 Harbin, China;* orcid.org/0000-0001-9590-3891; Phone: +86-451-82191204; Email: mchmchmchmch@163.com

Shouxin Liu − *Key Laboratory of Bio-based Material Science and Technology (Ministry of Education), College of Material Science and Engineering, Northeast Forestry University, 150040*

https://dx.doi.org/10.1021/acsomega.0c02016
ACS Omega 2020, 5, 22827−22839

Harbin, China; orcid.org/0000-0002-0491-8885; Phone: +86-451-82191204; Email: liushouxin@126.com; Fax: +86-451-82191502

Authors

Lihan Sun − *Key Laboratory of Bio-based Material Science and Technology (Ministry of Education), College of Material Science and Engineering, Northeast Forestry University, 150040 Harbin, China*

Mengru Wang − *Key Laboratory of Bio-based Material Science and Technology (Ministry of Education), College of Material Science and Engineering, Northeast Forestry University, 150040 Harbin, China*

Wei Li − *Key Laboratory of Bio-based Material Science and Technology (Ministry of Education), College of Material Science and Engineering, Northeast Forestry University, 150040 Harbin, China;* orcid.org/0000-0002-3008-9865

Sha Luo − *Key Laboratory of Bio-based Material Science and Technology (Ministry of Education), College of Material Science and Engineering, Northeast Forestry University, 150040 Harbin, China*

Yan Wu − *Key Laboratory of Bio-based Material Science and Technology (Ministry of Education), College of Material Science and Engineering, Northeast Forestry University, 150040 Harbin, China*

Complete contact information is available at: https://pubs.acs.org/10.1021/acsomega.0c02016

Author Contributions

†L.S. and M.W. contributed equally to this work.

Notes

The authors declare no competing financial interest.

■ ACKNOWLEDGMENTS

This work was funded by the National Natural Science Foundation of China (31890773) and the Fundamental Research Funds for the Central Universities (2572019BB02).

■ REFERENCES

(1) Roundhill, D. M.; Koch, H. F. Methods and techniques for the selective extraction and recovery of oxoanions. *Chem. Soc. Rev.* **2002**, *31*, 60−67.

(2) Alves, C. R.; de Buzin, P. J. W. K.; Heck, N. C.; Schneider, I. A. H. Utilization of ashes obtained from leather shaving incineration as a source of chromium for the production of HC-FeCr alloy. *Miner. Eng.* **2012**, *29*, 124−126.

(3) Zou, H.; Hu, E.; Yang, S.; Gong, L.; He, F. Chromium(VI) removal by mechanochemically sulfidated zero valent iron and its effect on dechlorination of trichloroethene as a co-contaminant. *Sci. Total Environ.* **2019**, *650*, 419−426.

(4) Guan, C.; Lv, X.; Han, Z.; Chen, C.; Xu, Z.; Liu, Q. The adsorption enhancement of graphene for fluorine and chlorine from water. *Appl. Surf. Sci.* **2020**, *516*, No. 146157.

(5) Zheng, M.; Zhao, X.; Wang, K.; She, Y.; Gao, Z. Highly Efficient Removal of Cr(VI) on a Stable Metal−Organic Framework Based on Enhanced H-Bond Interaction. *Ind. Eng. Chem. Res.* **2019**, *58*, 23330−23337.

(6) Yuan, W.; Xu, W.; Zhang, Z.; Wang, X.; Zhang, Q.; Bai, J.; Wang, J. Rapid Cr(VI) reduction and immobilization in contaminated soil by mechanochemical treatment with calcium polysulfide. *Chemosphere* **2019**, *227*, 657−661.

(7) Wan, Z.; Cho, D. W.; Tsang, D. C. W.; Li, M.; Sun, T.; Verpoort, F. Concurrent adsorption and micro-electrolysis of Cr(VI) by nanoscale zerovalent iron/biochar/Ca-alginate composite. *Environ. Pollut.* **2019**, *247*, 410−420.

(8) Xie, Y.; Lin, J.; Liang, J.; Li, M.; Fu, Y.; Wang, H.; Tu, S.; Li, J. Hypercrosslinked mesoporous poly(ionic liquid)s with high density of ion pairs: Efficient adsorbents for Cr(VI) removal via ion-exchange. *Chem. Eng. J.* **2019**, *378*, No. 122107.

(9) Sellami, F.; Senhadji, O. K.; Marais, S.; Colasse, L.; Fatyeyeva, K. Enhanced removal of Cr(VI) by polymer inclusion membrane based on poly(vinylidene fluoride) and Aliquat 336. *Sep. Purif. Technol.* **2020**, *248*, No. 117038.

(10) Luptakova, A.; Ubaldini, S.; Macingova, E.; Fornari, P.; Giuliano, V. Application of physical−chemical and biological−chemical methods for heavy metals removal from acid mine drainage. *Process Biochem.* **2012**, *47*, 1633−1639.

(11) Wu, Y.; Pang, H.; Liu, Y.; Wang, X.; Yu, S.; Fu, D.; Chen, J.; Wang, X. Environmental remediation of heavy metal ions by novel-nanomaterials: A review. *Environ. Pollut.* **2019**, *246*, 608−620.

(12) Ihsanullah Abbas, A.; Al-Amer, A. M.; Laoui, T.; Al-Marri, M. J.; Nasser, M. S.; Khraisheh, M.; Atieh, M. A. Heavy metal removal from aqueous solution by advanced carbon nanotubes: Critical review of adsorption applications. *Sep. Purif. Technol.* **2016**, *157*, 141−161.

(13) Ma, J.; Liu, C.; Chen, K. Removal of Cr(VI) species from water with a newly-designed adsorptive treatment train. *Sep. Purif. Technol.* **2020**, *234*, No. 116041.

(14) Xu, J.; Cao, Z.; Zhang, Y.; Yuan, Z.; Lou, Z.; Xu, X.; Wang, X. A review of functionalized carbon nanotubes and graphene for heavy metal adsorption from water: Preparation, application, and mechanism. *Chemosphere* **2018**, *195*, 351−364.

(15) Liu, G.; Abukhadra, M. R.; El-Sherbeeny, A. M.; Mostafa, A. M.; Elmeligy, M. A. Insight into the photocatalytic properties of diatomite@Ni/NiO composite for effective photo-degradation of malachite green dye and photo-reduction of Cr (VI) under visible light. *J. Environ. Manage.* **2020**, *254*, No. 109799.

(16) Kumar, A.; Jena, H. M. Adsorption of Cr(VI) from aqueous phase by high surface area activated carbon prepared by chemical activation with $ZnCl_2$. *Process Saf. Environ. Prot.* **2017**, *109*, 63−71.

(17) Zhong, Q.; Yue, Q.; Gao, B.; Li, Q.; Xu, X. A novel amphoteric adsorbent derived from biomass materials: Synthesis and adsorption for Cu(II)/Cr(VI) in single and binary systems. *ACS Omega* **2013**, *229*, 90−98.

(18) Butyrskaya, E. V.; Zapryagaev, S. A.; Izmailova, E. A. Cooperative model of the histidine and alanine adsorption on single-walled carbon nanotubes. *Carbon* **2019**, *143*, 276−287.

(19) Gusain, R.; Kumar, N.; Fosso-Kankeu, E.; Ray, S. S. Efficient Removal of Pb(II) and Cd(II) from Industrial Mine Water by a Hierarchical MoS_2/SH-MWCNT Nanocomposite. *ACS Omega* **2019**, *4*, 13922−13935.

(20) Knupp, W. G.; Ribeiro, M. S.; Mir, M.; Camps, I. Dynamics of hydroxyapatite and carbon nanotubes interaction. *Appl. Surf. Sci.* **2019**, *495*, No. 143493.

(21) Nashed, O.; Partoon, B.; Lal, B.; Sabil, K. M.; Shariff, A. M. Investigation of functionalized carbon nanotubes' performance on carbon dioxide hydrate formation. *Energy* **2019**, *174*, 602−610.

(22) Li, H.; Wu, W.; Hao, X.; Wang, S.; You, M.; Han, X.; Zhao, Q.; Xing, B. Removal of ciprofloxacin from aqueous solutions by ionic surfactant-modified carbon nanotubes. *Environ. Pollut.* **2018**, *243*, 206−217.

(23) Maciel, V. G.; Wales, D. J.; Seferin, M.; Ugaya, C. M. L.; Sans, V. State-of-the-art and limitations in the life cycle assessment of ionic liquids. *J. Clean. Prod.* **2019**, *217*, 844−858.

(24) Miao, Q.; Bi, E. Effects of soil components and solution inorganic cations on interactions of imidazolium-based ionic liquid with soils. *J. Environ. Manage.* **2018**, *223*, 975−983.

(25) Lawal, I. A.; Lawal, M. M.; Akpotu, S. O.; Okoro, H. K.; Klink, M.; Ndungu, P. Noncovalent Graphene Oxide Functionalized with Ionic Liquid: Theoretical, Isotherm, Kinetics, and Regeneration Studies on the Adsorption of Pharmaceuticals. *Ind. Eng. Chem. Res.* **2020**, *59*, 4945−4957.

(26) Salar-García, M. J.; Ortiz-Martinez, V. M.; Hernandez-Fernandez, F. J.; de Los Rios, A. P.; Quesada-Medina, J. Ionic liquid

technology to recover volatile organic compounds (VOCs). *J. Hazard. Mater.* **2017**, *321*, 484−499.
(27) Zhang, G.; Etzold, B. J. M. Ionic liquids in electrocatalysis. *J. Energy Chem.* **2016**, *25*, 199−207.
(28) Zhang, M.; Ma, X.; Li, J.; Huang, R.; Guo, L.; Zhang, X.; Fan, Y.; Xie, X.; Zeng, G. Enhanced removal of As(III) and As(V) from aqueous solution using ionic liquid-modified magnetic graphene oxide. *Chemosphere* **2019**, *234*, 196−203.
(29) Disasa Irge, D. Ionic Liquids: A Review on Greener Chemistry Applications, Quality Ionic Liquid Synthesis and Economical Viability in a Chemical Processes. *Am. J. Phys. Chem. A* **2016**, *5*, 74−79.
(30) Singhal, S.; Agarwal, S.; Singh, M.; Rana, S.; Arora, S.; Singhal, N. Ionic liquids: Green catalysts for alkene-isoalkane alkylation. *J. Mol. Liq.* **2019**, *285*, 299−313.
(31) Wasilewski, T.; Gębicki, J.; Kamysz, W. Prospects of ionic liquids application in electronic and bioelectronic nose instruments. TrAC-Trends. *Anal. Chem.* **2017**, *93*, 23−36.
(32) Vafaeezadeh, M.; Alinezhad, H. Brønsted acidic ionic liquids: Green catalysts for essential organic reactions. *J. Mol. Liq.* **2016**, *218*, 95−105.
(33) He, Z.; Alexandridis, P. Ionic liquid and nanoparticle hybrid systems: Emerging applications. *Adv. Colloid. Interface Sci.* **2017**, *244*, 54−70.
(34) Zhitkovich, A. Chromium in Drinking Water: Sources, Metabolism, and Cancer Risks. *Chem. Res. Toxicol.* **2011**, *24*, 1617−1629.
(35) Ahmadpour, A.; Eftekhari, N.; Ayati, A. Performance of MWCNTs and a low-cost adsorbent for Chromium(VI) ion removal. *J. Nanostruct. Chem.* **2014**, *4*, 171−178.
(36) Wang, J.; Yin, X.; Tang, W.; Ma, H. Combined adsorption and reduction of Cr(VI) from aqueous solution on polyaniline/multi-walled carbon nanotubes composite. *Korean J. Chem. Eng.* **2015**, *32*, 1889−1895.
(37) Lee, C. G.; Kim, S. B. Cr(VI) Adsorption to Magnetic Iron Oxide Nanoparticle-Multi-Walled Carbon Nanotube Adsorbents. *Water Environ. Res.* **2016**, *88*, 2111−2120.
(38) Hu, J.; Chen, C.; Zhu, X.; Wang, X. Removal of chromium from aqueous solution by using oxidized multiwalled carbon nanotubes. *J. Hazad. Mater.* **2009**, *162*, 1542−1550.
(39) Wu, H.; Lu, W.; Chen, Y.; Zhang, P.; Cheng, X. Application of Boehm Titration for the Quantitative Measurement of Soot Oxygen Functional Groups. *Energy Fuels* **2020**, *34*, 7363−7372.
(40) Boehm, H. P. Some aspects of the surface chemistry of carbon blacks and other carbons. *Carbon* **1994**, *32*, 759−769.

https://dx.doi.org/10.1021/acsomega.0c02016
ACS Omega 2020, 5, 22827−22839